ASEAN Engineering Journal

Full Paper

DRAG REDUCTION OF A SIMPLIFIED TRUCK MODEL USING CAB ROOF FAIRINGS

Nurul Syamimi Zahirah Ismadi, Ahmad Fikri Mustaffa*

School of Mechanical Engineering, Engineering Campus, Universiti Sains Malaysia, 14300, Nibong Tebal, Penang, Malaysia

Article history
Received
30 September 2022
Received in revised form
24 March 2023
Accepted
27 March 2023
Published online
30 November 2023

*Corresponding author
afikri@usm.my

Graphical abstract

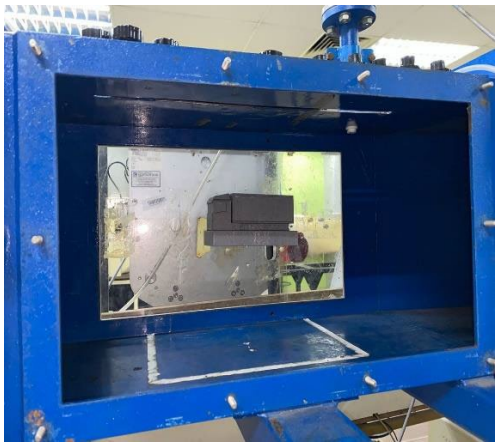

Abstract

Adverse effects of climate change have prompt transition towards a low-carbon transportation sector. Electrification of the transportation sector is one of the ongoing efforts to reduce the Greenhouse Gas emissions. However, electrification of long haul and heavy-duty vehicles remain a huge challenge due to cost and limitation in the current battery technology. Improving the aerodynamic design of current truck-trailer is an alternative to electrification. This initiative involves modifying the current truck-trailer body design or attaching accessories for aerodynamic drag reduction that can lead to improved fuel economy. In this paper, the effectiveness of four Cab Roof Fairing (CRF) designs on the aerodynamic drag reduction of a simplified truck model is investigated. The results of a numerical simulation performed on a two-dimensional model show that the CRF can reduce aerodynamic drag by up to 45%. The CRF is found to reduce the vertical velocity component of the flow at fore part of the truck body. This leads to a relatively smaller wake region when compared against the baseline case. Wind tunnel results is performed to verify the results of the numerical simulation. At Reynolds number $\approx 1 \times 10^5$, the measured coefficient of drag reduction is about 6% when compared with the baseline case.

Keywords: Aerodynamics, Flow control, CFD, Wind Tunnel, Drag

1.0 INTRODUCTION

Malaysia aspires to become a carbon neutral country by the year 2050. One of the main sources of green house gas (GHG) emissions is the transport sector. The transport sector consumes about 40% of the total energy consumption in Malaysia[1]. The road transport sector which accounts for the largest portion of the transportation sector includes cars, motorcycles and heavy duty vehicles such as trucks. It is reported that 85% of the GHG emissions comes from the transport sector [2].

Electrification of the road transport sector is one stragety to reduce the GHG emissions. Electrification means that electric powertrains replace conventional internal combustion engines for vehicle propulsion. The global demand for electric vehicles (EV) for passenger cars has shown a steady increase in the past years. This reflects the consumer confidence towards the current EV in terms of cost and reliability. In the ASEAN region, the sales of green vehicles achieved 32% of the total vehicles sold in 2018 [3]. Despite the popularity of EV for passenger cars, electrification of long haul heavy duty vehicles remains a huge challege in terms of cost and battery technology [4], [5].

The effort to improve the fuel efficiency of heavy-duty trucks has been explored in the USA and Europe. The Department of Environment (DOE), USA, initiated a research project to reduce the fuel consumption of Class 8 trailer-trucks that consumes about 11-12% of the total US fuel usage [6]. The DOE initiative aimed to reduce the aerodynamic drag of trailer-truck by 25% which translates to 12% reduction of the fuel economy. This initiative combined computational and experimental work to find innovative ways to reduce aerodynamic drag by improving the aerodynamic design of the truck-trailers. The European Union (EU) launched a similar initiative to improve the fuel economy of trailer and trucks. The project is called the

Configurable and Adaptable Trucks and Trailers for Optimal Transport Efficiency (TRANSFORMERS) [7], [8]. One of the initiatives of the project involves introducing aerodynamic truck features to reduce drag and improve fuel efficiency. The goal of the project is to reduce the overall energy consumption by 25% per tonne-km of the freight transport. It is reported that improving the aerodynamic design of the trailer can achieve 5.7% fuel consumption at 80 kilometers per hour.

In general, there are three regions where the aerodynamic design of the truck can be improved; the upper part of the truck, the underbody of the truck-trailer and the rear body of the trailer. Roof fairings are added to trucks to improve the air flow forebody region of the truck. Kim et al. [9] conducted wind tunnel experiments to investigate the feasibility of roof-fairings to reduce aerodynamic drag. The test was conducted for a scaled-down model of a 15-tonne truck. The test result shows that the cab roof fairing reduces the drag coefficient by 19%. In a different study, a bio-inspired cab roof fairing design is tested in a wind tunnel for the same truck model[10]. The drag coefficient is reduced by 20%. Charles and Yang [11] investigated the effectiveness of cross-flow vortex trap device (CVTD) inside the trailer-truck gap region. Numerical simulation results show that the CVTD can achieve a drag reduction of about 24%. Story et al. [12] tested the effect of CVTD on the aerodynamic drag in a wind tunnel experiment. The test is performed for a scaled-down model at a Reynolds number of 900,000. It is reported that the CVTD can reduce the aerodynamic drag by 12%.

The clearance height between the underbody and ground is another area where design improvements can be considered for more fuel-efficient truck designs. Castelain et al. [13] investigated the influence of truck underbody velocity on the wake structure at the rear body. Four classes of wake structures are identified when the underbody velocity varies. When the underbody velocity is above 60% of the freestream velocity, the rear wake structure mimics a bluff body where no clearance height exists. This is not the case for truck-trailers. When the underbody velocity is relatively smaller than the free-stream velocity, the low momentum underbody flow detaches from the ground to generate wake features that contribute to the overall aerodynamic drag. Landman et al. [14] showed that adding a side skirt that covers the wheels of the truck can achieve drag reduction of up to 19% of the baseline case when no skirt is added to the truck. The clearance height of the truck and ground is approximately 8mm when the skirt is attached. Wind tunnel tests by Kim and Lee [15] show that the skirt can reduce drag by 6%. Experiments by Stephens and Babinsky [16] suggest that the skirt prevents higher momentum flow from entering the upper half of the body from the sides. Adding the side skirt also have detrimental effects that leads to additional drag due to the interaction with the near-ground flow. The skirting clearance height needs to be optimized to avoid detrimental effects due to the near ground flow interaction that can offset the overall drag reduction mechanism.

Modifications to the rear part of the trailer has shown great potential in reducing aerodynamic drag. NASA began studying boat tail design for trailers since the 1970's [17]. Test results show that the boat tail design can reduce up to 32% aerodynamic drag as compared to the baseline design. Wind tunnel result in [18], [19] further show the potential of rear trailer devices in reducing drag. The rear trailer devices are shown to perform the best with combinations with the device attached at the front and the side of the trailer. Rejniak and Gatto [20] explained that the trailing edge devices modifies the structure of the generated wake which results in aerodynamic drag reduction.

This paper demonstrates the integration of numerical simulations, rapid prototyping and wind tunnel testing in the design process of a truck-trailer cab roof fairing (CRF) for aerodynamic drag reduction. Wind tunnel model design and testing are known to be expensive to fabricate and time consuming. Numerical simulations on the other hand are fast and relatively cheap compared to wind tunnel testing. However, numerical simulations may lack accuracy hence requires experimental data for validation and verification. The advent of rapid prototyping has allowed researchers and designers to combine numerical simulations and wind tunnel testing at a relatively lower cost. The design process of CRF is initiated by using numerical simulations in order to identify the roof-fairing design that reduces the maximum aerodynamic drag. The reference case and best-case model from the numerical simulations are then fabricated using rapid prototyping. The models are then tested in a wind tunnel for verification of the numerical simulation results.

2.0 METHODOLOGY

2.1 Geometry and Numerical Method

Figure 1 shows the simplified baseline model of the truck-trailer and four CRF configurations. Four CRF designs, CRF1, CRF2, CRF3 and CRF4 are generated using CAD software. The CRF configurations are designed based on existing CRF design in the market. Only four CRF designs are considered because these designs represent the most used CRF designs in Malaysia. The length, L, of the model is 14 m with a maximum height, h, of 3.9 m. The gap between the truck and trailer is 0.2 m for all the configurations. Steady two-dimensional RANS equations are solved using commercial CFD software, ANSYS Fluent 2022. The pressure field is solved by coupling of the momentum equation and the continuity equation. Values at the cell boundary are interpolated from cell center values using a Second Order Upwind method. The solution is marched to a steady state using a pseudo-time stepping approach. A k-ω SST model is chosen as the turbulence model.

The computation domain and mesh are shown in Figure 2. The computation domain has a size of $6L \times 7.5h$. The model truck is located at the center of the computational domain. Unstructured hexahedral meshes are generated for the computational domain. Near the walls, a Y+ less than 2 criteria is prescribed. The total number of grids points generated for this 2D domain is about 6100. At the inlet, a velocity inlet of 20 m/s is specified. The outlet condition is set to atmospheric pressure. Adiabatic and no-slip condition are applied to the upper and lower walls. The calculations are run for at least 500 iterations. The solutions are considered to converged when the all the residuals fall below a value of 10^{-4} or stabilises for at least the last 100 iterations.

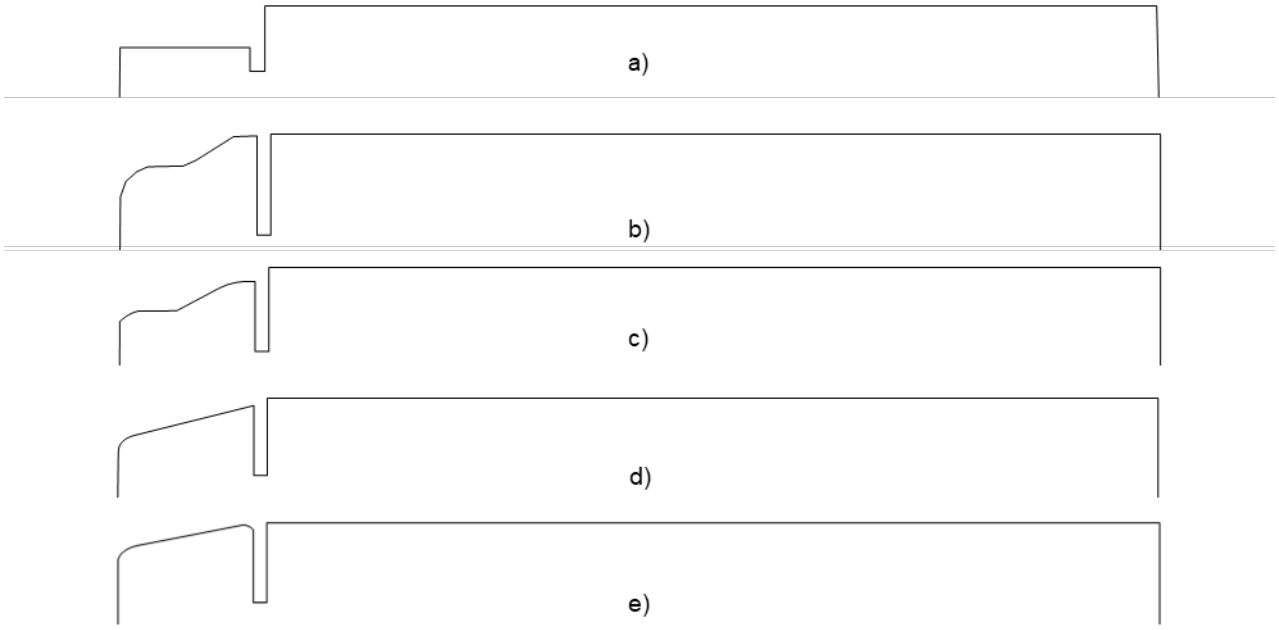

Figure 1 a) Baseline model and four cab roof fairing configurations: b) CRF1 c) CRF2 d) CRF3 e) CRF4

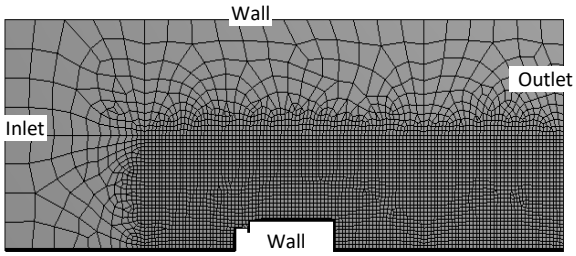

Figure 2 Computational domain and mesh

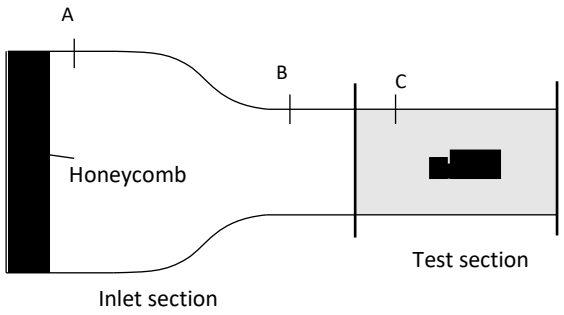

Figure 3 Cross-section of the subsonic wind tunnel

2.2 Wind Tunnel Test Setup

The wind tunnel used in this study is an open circuit subsonic wind tunnel located at Universiti Sains Malaysia. Figure 3 shows the meridional view of the fore part of the wind tunnel. The inlet section consists of honeycomb flow straighteners and a contraction cone. The contraction ratio is 9:1. The test section is a square duct with a dimension of 300 mm × 300 mm. The length of the test section is 600 mm. The flow velocity into the inlet section of the wind tunnel is measured by calculating the static pressure difference across the contraction section. Static pressure readings are measured at point A and B using a differential manometer. Four static pressure tapings are located 90° apart at locations A and B. Ideally, the flow velocity into the inlet section of the wind tunnel, V_{in}, equals the velocity into the test section, V_{test}. However, discrepancy exist due to total pressure loss from flow contraction and boundary layer effects. Hence, the wind tunnel is calibrated prior to testing in order to find the relationship between V_{in} and V_{test}. V_{test} is measured at the entrance of the test section, point C, using a pitot-static tube. The pitot-static tube is inserted at the midpoint of the test section. V_{in} is varied by varying the wind tunnel fan speed. The pressure readings at point A, B and C are recorded to calculate V_{in} and V_{test}.

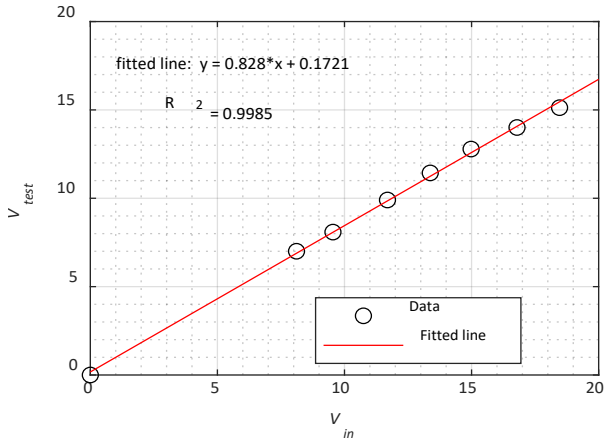

Figure 4 Wind tunnel calibration plot

Figure 4 shows the relationship between V_{in} and V_{test}. Through this plot, desired V_{test} can be obtained from the corresponding

static pressure difference across the contraction section. The drag is measured using a three-component balance (TecQuipment) as shown in Figure 5a). As shown in Figure 5b) The truck model is mounted to the force balance using a custom-made shaft. The component balance is calibrated by attaching blocks of known mass on to the balance. The calibration plot is shown in Figure 6. Drag measured by the force balance is corrected using the calibration plot obtained.

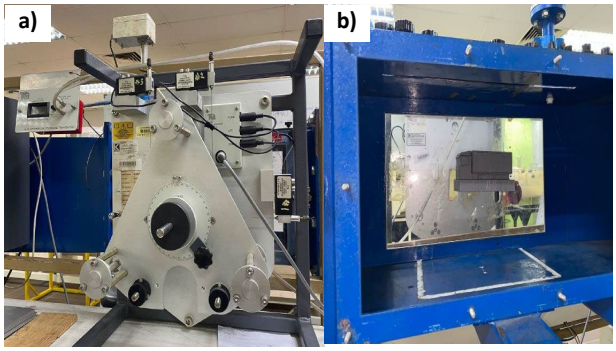

Figure 5 a) Three component force balance and b) model truck mounted to the force balance.

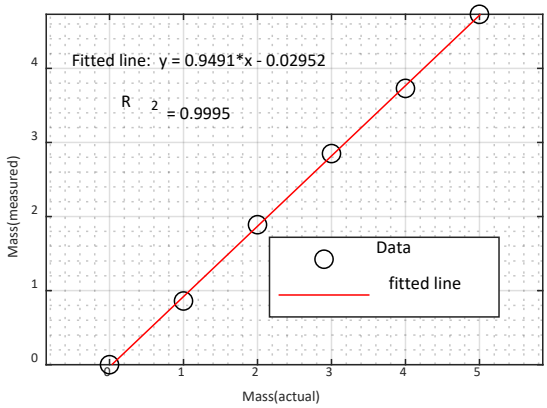

Figure 6 Force balance calibration plot

3.0 RESULTS AND DISCUSSION

3.1 Numerical Simulation Results

The drag force, D, is calculated using a control volume analysis whereby it is assumed that the flow is steady, inviscid and incompressible. The drag force, D, is calculated using Eq. 1.

$$D = \int_0^H \rho V_2 (V_\infty - V_2)\, w dy \qquad \text{(Eq. 1)}$$

Here, ρ is the air density with a value of 1.22 $\frac{kg}{m^3}$. V_∞ and V_2 are the inlet velocity and the downstream velocity at about $0.5L$ aft of the model truck tail. w, y, and H are the model width, vertical position and domain height, respectively. Figure 7 shows the V_2 profile for all the models simulated. The V_2 profile is normalized by the V_∞. The baseline case represented by open circles has a relatively larger deficit region as compared to all the other models. The deficit region is caused by the blockage effect due to the model body. The blockage causes the flow to be radially displaced and as a result, the normalized V_2 profiles is shown to have a relative higher V_∞ ($\frac{V_2}{V_\infty} > 1$) from about $0.2H$ to H.

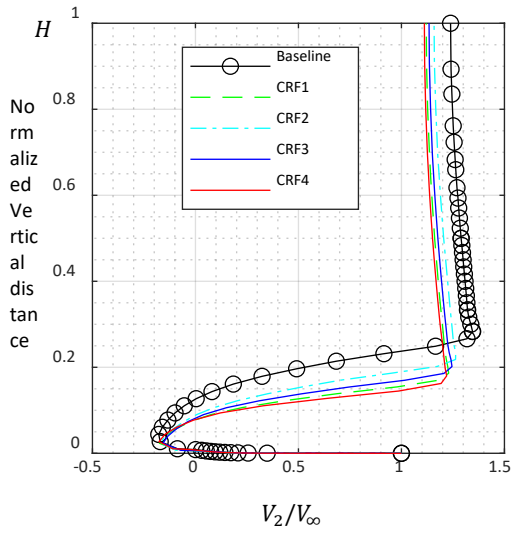

Figure 7 Normalized V_2 profile at $0.5L$ aft of the model truck tail

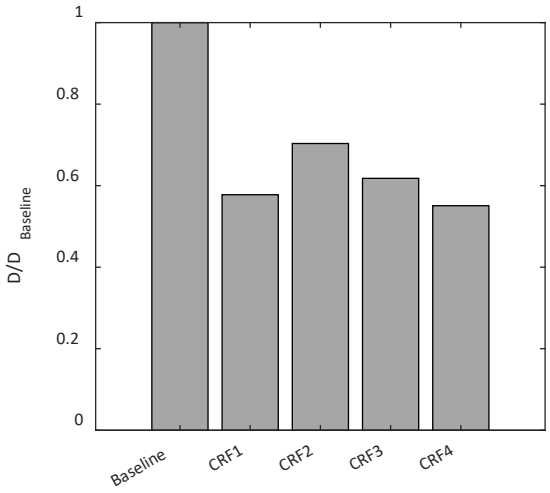

Figure 8 Calculated drag values using Eq.1

The size of deficit region is related to the D as shown in Figure 8. Here, the D values are normalized by the baseline case drag force, $D_{Baseline}$. It is shown the CRF helps to reduce the drag force as compared to the baseline case. CRF4 has the largest drag force reduction in comparison all the other cases. The normalized value of D for CRF4 is 0.55 whereas CRF1, CRF2 and CRF3 have a value of 0.58, 0.70, and 0.62, respectively.

Figure 9 shows the distribution of vertical velocity, V_y, normalized by the V_∞. Since the V_∞.is purely axial, any deficit in V_∞ is distributed in the vertical direction. Blue regions in the contour plot show high values of V_y. This is visible at the fore part of the truck as the flow navigates itself across the model body. The baseline case shows a relatively larger area of high V_y as compared to the other cases with CRF. Case CRF4 with the lowest D shows a relatively smaller region of high V_y.

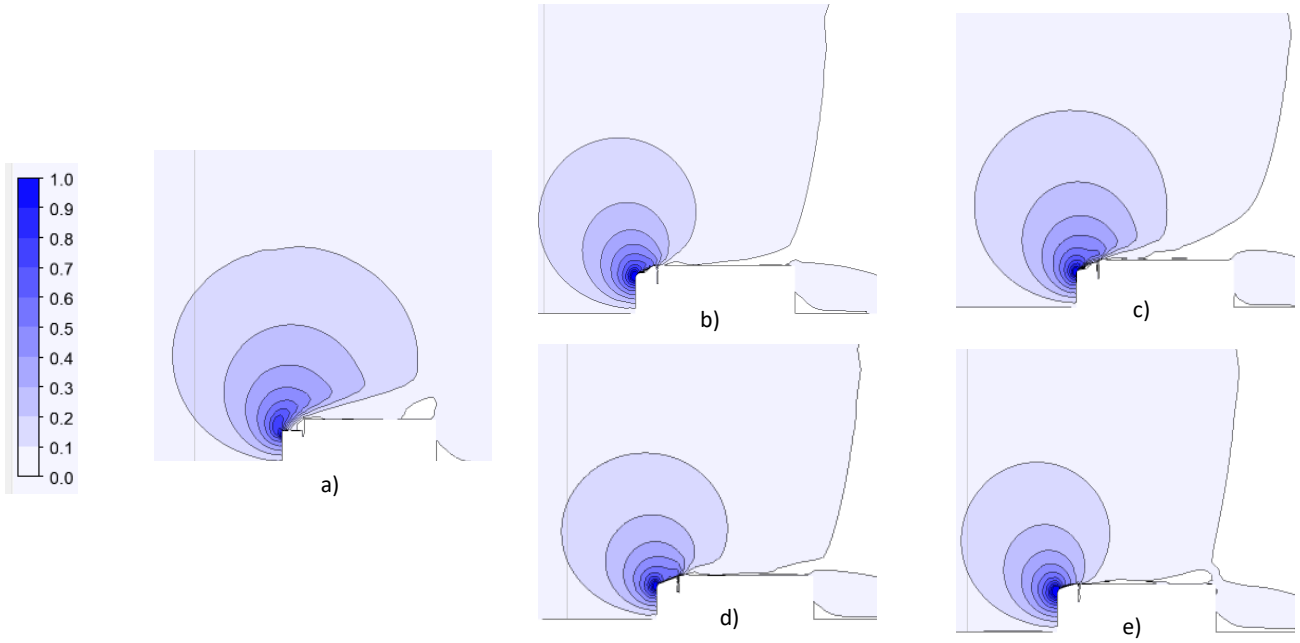

Figure 9 Distribution of V_y value for a) baseline, b) CRF1, c) CRF2, d) CRF3, and e) CRF4

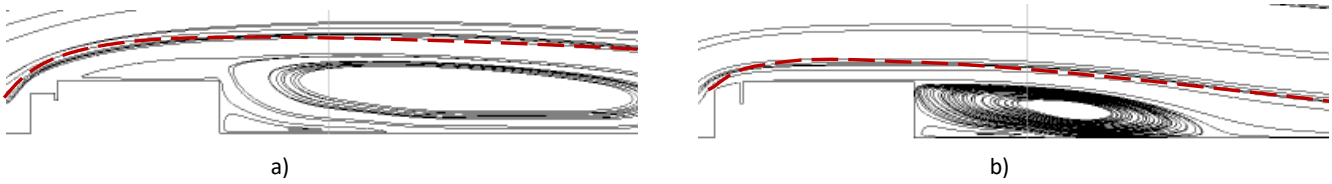

Figure 10 Streamlines across the model body a) baseline case and the case with highest drag reduction, b) CRF4. Dashed red line shows the boundary of the wake region.

The CRF reduces the D by reducing the areas of large V_y that occurs at the fore part of the truck body. The influence of the V_y region on the truck body aft region is shown in Figure 10. The streamlines across the model geometry are compared for the baseline case and the case with highest drag reduction, case CRF4. The red dashed line shows the boundary of the wake region that develops as the flow passes through the model geometry. The size of the wake region is larger for the baseline case as compared to case CRF4. This explains the relatively larger velocity deficit for the baseline case as compared to the other CRF cases as shown in Figure 7. The role of CRF in reducing drag is clearly demonstrated from this streamline plot. As the flow passes through the fore part of the truck, the CRF guides the flow so that the vertical component of the velocity, V_y, is minimized This helps to reduce the size of the wake region that forms downstream of the truck body.

Figure 11 shows the distribution of the static pressure coefficient, c_p, of the baseline case and CRF4 along the trailer body. The c_p is defined in Eq. 2. The numerator is the pressure difference between the pressure on the trailer surface and the freestream pressure. The denominator is the dynamic pressure. For incompressible flow, the c_p, can be defined using the only the velocity ratio of the flow near the trailer body to the free stream velocity. In this case, the freestream velocity is the inlet velocity. If c_p is 1, this means that flow velocity close to the body is to zero. On the other hand, if $c_p = 0$, this means that the flow velocity close to the body is equal to the freestream velocity. For the Baseline case, the c_p, is close to 1 throughout the trailer body. This indicates that the flow velocity,v, in that region is relatively lower than the freestream velocity, V_∞. A relatively lower velocity contributes to the drag force as the c_p is relatively high. For CRF4, the c_p distribution is close to 1 at the front part of the body and gradually reduces along the trailer body. This explains why CRF4 has a relatively lower aerodynamic drag than the baseline case.

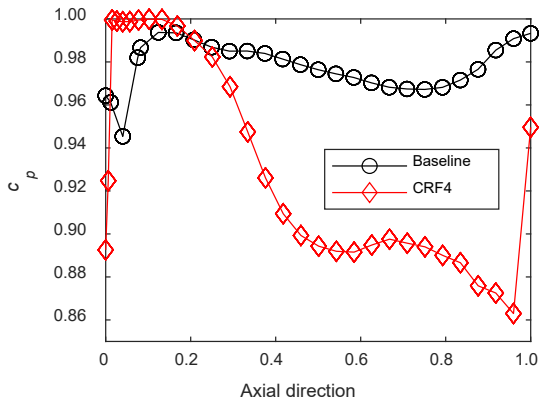

Figure 11 Static pressure distribution along trailer for a baseline and CRF4 cases

$$c_p = \frac{P - P_\infty}{0.5\rho V_\infty^2} = 1 - \left(\frac{v}{V_\infty}\right)^2 \quad \text{(Eq. 2)}$$

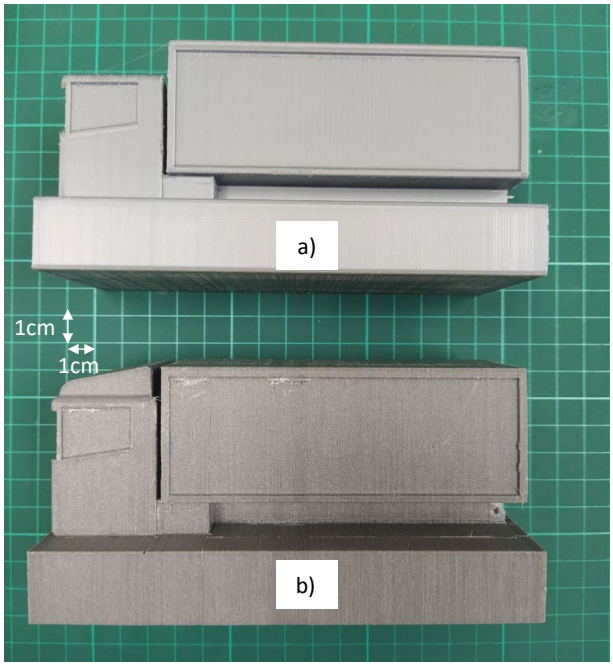

Figure 12 3D printed truck model of a) Baseline and b) CRF4

3.2 Wind Tunnel Test Result

A wind tunnel test is performed to verify the findings of the numerical results. The model geometry for the baseline case and CRF4 are fabricated using a 3D printer as shown in Figure 12. Due to the size limitation and wind speed of the wind tunnel, the Reynolds number of model and actual truck cannot be matched to achieve dynamic similarity. The actual truck Reynolds number is in the order of magnitude of 10^6. Therefore, the length of the 3D printed model is determined by fixing the Reynolds number to 1×10^5. The order of magnitude of the Reynolds number is comparable to the wind tunnel tests performed in [9] and [10]. The flow regime at this order of magnitude is turbulent flow is sufficient to capture the flow physics of the actual truck Reynolds number despite not able to match the actual Reynolds number.

Figure 13 shows the result of the wind tunnel test. The horizontal axis is the Reynolds number and vertical axis is the coefficient of drag, c_d, as defined in Eq. 2.

$$c_d = \frac{2D}{\rho V_{test}^2 A} \quad \text{(Eq. 3)}$$

The drag force, D, measurements are obtained from the calibrated force balance. The truck model frontal area, A, is obtained from CAD software when preparing the geometry drawing. The air density, ρ, is assumed to be constant throughout the test velocity since the variation in the measured room air temperature is small. The velocity in the test section, V_{test}, is determined using the calibration plot shown in Figure 4. The c_d for CRF4 is relatively smaller than the baseline case throughout the test Reynolds, Re, number range. The change of c_d change between baseline and CRF4 is plotted in Fig. 14. At $Re = 0.4 \times 10^5$, the Δc_d is about 30% and when $Re = 1.4 \times 10^5$, the Δc_d is about 6%.

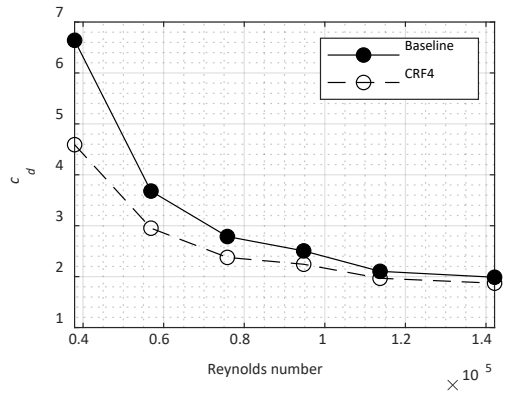

Figure 13 Measured aerodynamic drag of the truck model at different Reynolds number order of magnitude.

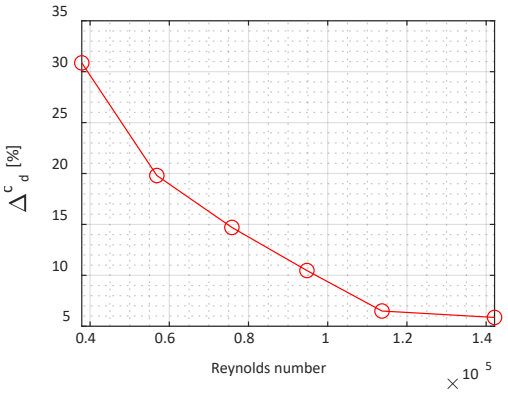

Figure 14 The change of drag coefficient of the truck model at different Reynold number between baseline and CRF4

4.0 CONCLUSION

Numerical simulations are performed on a simplified two-dimensional model truck to investigate the effectiveness of CRF in reducing drag. The results of the two-dimensional numerical simulations show that the CRF can reduce drag up to 45% as compared to the baseline case. The drag reduction mechanism is attributed to the reduction of the vertical velocity component size distribution at the fore part of the truck. The CRF acts as a guide for the flow across the truck body. The reduction in the vertical velocity component is found to reduce the size of the wake are that is responsible for the aerodynamic drag. A relatively smaller wake region leads to aerodynamic drag reduction. The result of the simulation is verified and validated by fabricating a scaled-down truck model using rapid prototyping technology. This method allows for the model to be fabricated fast at a relatively lower cost compared to traditional method. Wind tunnel test of the most effective CRF (CRF4) shows a 6% drag reduction at $Re = 1.4 \times 10^5$.

Acknowledgement

The authors would like to thank Universiti Sains Malaysia for funding the wind tunnel test under the Short-Term Grant 304/PMEKANIK/6315582.

References

[1] Suruhanjaya Tenaga. 2021. *Malaysia Energy Statistics Handbook 2020,* Suruhanjaya Tenaga, Malaysia,

[2] S. I. Mustapa and H. A. Bekhet, 2016, "Analysis of CO2 emissions reduction in the Malaysian transportation sector: An optimisation approach," *Energy Policy*, 89: 171–183, doi: 10.1016/j.enpol.2015.11.016.

[3] National Automotive Policy 2020, Ministry of International Trade and Industry, Malaysia,

[4] B. Nykvist and O. Olsson, 2021, "The feasibility of heavy battery electric trucks," *Joule*, 5(4): 901–913, doi: 10.1016/j.joule.2021.03.007.

[5] R. Vijayagopal and A. Rousseau, 2021 "Electric truck economic feasibility analysis," *World Electric Vehicle Journal*, 12(2): 75, doi: 10.3390/wevj12020075.

[6] R. McCallen *et al.*, 2007. "*DOE Project on Heavy Vehicle Aerodynamic Drag,*" Livermore, CA (United States). doi: 10.2172/1036846.

[7] A. Hariram, T. Koch, B. Mårdberg, and J. Kyncl, 2019, "A study in options to improve aerodynamic profile of heavy-duty vehicles in Europe," *Sustainability (Switzerland)*, 11(19): 5519. doi: 10.3390/su11195519.

[8] P. Adams *et al.*, "*Transformers-Configurable and Adaptable Trucks and Trailers for Optimal Transport.*" [Online]. Available: www.transformers-project.eu Retrieved on 25 September 2021

[9] J. J. Kim, S. Lee, M. Kim, D. You, and S. J. Lee, 2017 "Salient drag reduction of a heavy vehicle using modified cab-roof fairings," *Journal of Wind Engineering and Industrial Aerodynamics*, 164: 138–151, doi: 10.1016/j.jweia.2017.02.015.

[10] J. J. Kim, J. Hong, and S. J. Lee, 2017 "Bio-inspired cab-roof fairing of heavy vehicles for enhancing drag reduction and driving stability," *International Journal of Mechanical Science*. 131–132: 868–879, doi: 10.1016/j.ijmecsci.2017.08.010.

[11] T. Charles and Z. Yang, 2022 "Comparison of the Effectiveness of Drag Reduction Devices on a Simplified Truck Model through Numerical Simulation," *Modelling*, 3(3): 300–313. doi: 10.3390/modelling3030019.

[12] J. Story, I. V. Garcia, and H. Babinsky. 2021. "The Effect of Cross-Flow Vortex Trap Devices on the Aerodynamic Drag of Road Haulage Vehicles," *SAE Technical Paper*, 2021-01-5040,10, doi: 10.4271/2021-01-5040.

[13] T. Castelain, M. Michard, M. Szmigiel, D. Chacaton, and D. Juvé, 2018, "Identification of flow classes in the wake of a simplified truck model depending on the underbody velocity," *Journal of Wind Engineering and Industrial Aerodynamics*, 175: 352–363, doi: 10.1016/j.jweia.2018.02.004.

[14] D. Landman, R. Wood, W. Seay, and J. Bledsoe, 2010, "Understanding practical limits to heavy truck drag reduction," *SAE International Journal of Commercial Vehicles.* 2(2): 183–190, doi: 10.4271/2009-01-2890.

[15] J. J. Kim and S. J. Lee, 2017, "Drag-reducing underbody flow of a heavy vehicle with side skirts," *Journal of Visualization.* 20(2): 369–378. doi: 10.1007/s12650-016-0401-7.

[16] R. G. Stephens and H. Babinsky, 2016 "An Experimental Study on Truck Side-Skirt Flow," *SAE International Journal of Passenger Cars - Mechanical Systems*, 9(2): 2016-01–1593, doi: 10.4271/2016-01-1593.

[17] R. L., Peterson, 1981. "Drag reduction obtained by the addition of a boat-tail to a box shaped vehicle,", NASA Contractor Report 163113. Dryden Flight Research Center.

[18] T. Skrucany, B. Sarkan, and J. Gnap, 2016. "Influence of aerodynamic trailer devices on drag reduction measured in a wind tunnel," *Eksploatacja i Niezawodnosc*, 18(1): 151–154, doi: 10.17531/ein.2016.1.20.

[19] L. Salati, P. Schito, and F. Cheli, 2017. "Wind tunnel experiment on a heavy truck equipped with front-rear trailer device," *Journal of Wind Engineering and Industrial Aerodynamics*, 171: 101–109, doi: 10.1016/j.jweia.2017.09.016.

[20] A. Anna Rejniak and A. Gatto, 2021, "On the drag reduction of road vehicles with trailing edge-integrated lobed mixers," *Proceedings of the Institution of Mechanical Engineers, Part D: Journal of Automobile Engineering*, 236(7): 1515-1545 doi: 10.1177/09544070211039697.